DYNAMIC MODELING AND ANALYSIS OF MOTORIZED MILLING SPINDLES FOR OPTIMIZING THE SPINDLE CUTTING PERFORMANCE

Dr. Sinan Badrawy, Engineering Manager
Moore Nanotechnology Systems, LLC

ABSTRACT

Future machine tools have to be highly dynamic systems to sustain the required productivity, accuracy and reliability. Both the machine tool system and the spindle system (Spindle/Tool-holder/Tool) are necessary to be optimized for their usability or cutting performance to meet the productivity and availability requirements of the end user. However, in industrial practice, the availability of a machine system is significantly influenced by the spindle cutting performance and its reliability. The focus of this paper is to show a design methodology for optimizing the dynamic cutting performance of spindles by establishing the relationship between the required cutting parameters and the basic design principles of a spindle/tool-holder/tool system. In addition, the influence of the spindle cutting performance, which is determined by the tooling parameters (such as spindle/tool holder interface, tool holder mass, etc.) will be shown in this paper.

NOMENCLATURE

b_{cr}	[mm]	Critical axial depth of cut
c	[Ns/mm]	Viscose damping
c_M	[cm^3/min/kW]	Material cutting factor
D_{Tool}	[mm]	Tool diameter
F	[N]	Force
f_n	[Hz]	Natural frequency
f_R	[Hz]	Resonance frequency
f_z	[mm/rev]	Chip per tooth
$G(j\omega)$	[mm/N]	Dynamic transfer function
k	[N/mm]	Stiffness
k_{cb}	[N/mm^2]	Specific dynamic cutting coefficient
MRR_{cr}	[cm^3/min]	Critical material removal rate
n_{Base}	[rpm]	Spindle base speed
P_{cr}	[kW]	Critical machining power
P_{S1}	[kW]	Continuous spindle power
S_{pe}	--	Spindle cutting performance factor
Y	[mm]	Displacement response
z	--	Number of teeth
z_{avg}	--	Average number of teeth in cut
ξ	--	Damping ratio
μ	--	Machining overlapping factor (for milling $\mu = 1$)

INTRODUCTION

Two common test methods for evaluating the cutting performance of spindles and machine tool systems are being applied in industry today [1, 2, 3, 4]. The first method determines the availability of the specified continuous P_{S1} rated spindle power over a given speed range through performing horsepower cuts. The second method is to predict or perform a variety of test cuts with a defined tool and workpiece material to determine the chatter free cutting speed zones (lubing diagrams) and their critical axial depth of cut [5, 6, 7, 8]. However, both of these methods are influenced by a variety of cutting parameters, such as tool wear conditions, tool geometry, etc. Neither of these methodologies can establish a direct comparison of the cutting performance between different spindle designs nor can they be applied in the conceptual design phase of the machine tool and/or the spindle system.

In order to compare different milling spindle designs or concepts independently from their application requirements as well as their power and speed characteristics, a methodology has to be established which allows defining the amount of the available spindle power that can be utilized for chip removal under no chatter conditions at any given spindle speed. In other words, the spindle cutting performance S_{pe} can be defined as the ratio between the critical machining power P_{cr} which can be utilized for chip removal, chatter free, at the spindle base speed n_{Base} for a given workpiece material, and the available continuous spindle power P_{S1}:

$$S_{pe} = \frac{P_{cr}}{P_{S1}} \qquad (1)$$

The critical machining power P_{cr} is determined with:

$$P_{cr} = MRR_{cr}.c_M \qquad (2)$$

while the Critical Material Removal Rate (MRR_{cr}) is:

$$MRR_{cr} = b_{cr}.f_z.z.n_{Base}.D_{Tool} \qquad (3)$$

Table 1 shows the values for some material cutting factors c_M which are commonly machined.

Material	c_M [cm³/min/kW]	k_{cb} [N/mm²]
Aluminum	70	83
Gray Cast Iron	40	200
Alloy Steel	30	355
Titanium	25	387

Table 1: Examples for c_M and k_{cb} values for commonly machined materials

The critical axial depth of cut value b_{cr} is determined through the maximum negative real part $Re_{max}\{G(j\omega)\}_{neg}$ of the dynamic transfer function of a spindle/tool-holder/tool system (Figure 1) [5]. This value reflects a chatter free cutting condition across the entire spindle speed range of a spindle/tool-holder/tool system. The well known stability lobe diagram, which predicts the

Re{G_g(jf)}

0

-1.00 × 10⁻⁰⁴

-2.00 × 10⁻⁰⁴

-3.00 × 10⁻⁰⁴
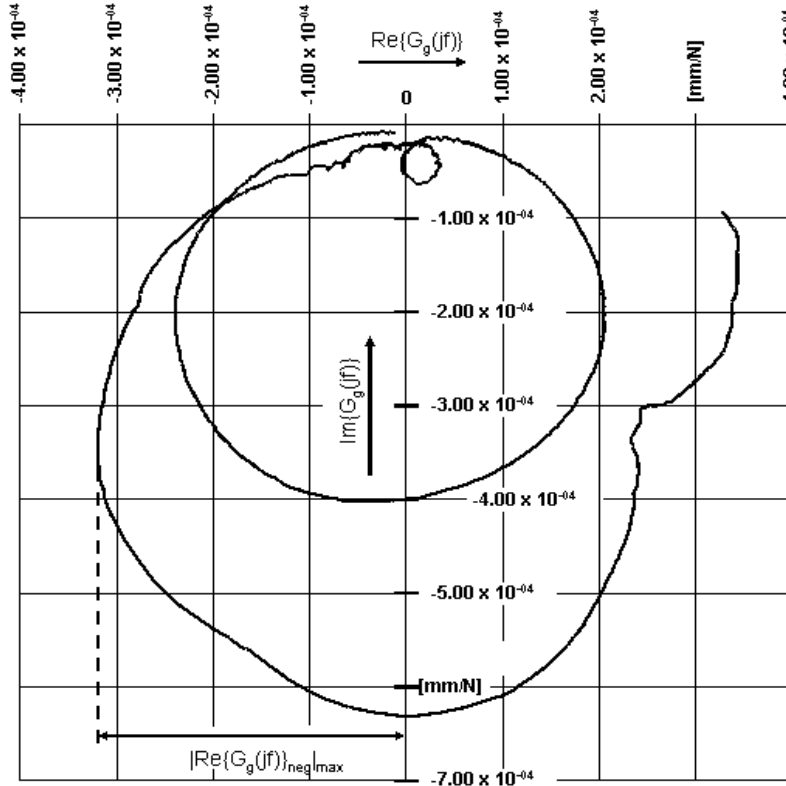
-4.00 × 10⁻⁰⁴

-5.00 × 10⁻⁰⁴

[mm/N]

-7.00 × 10⁻⁰⁴

Figure 1: Example of the maximum negative real part of a dynamic transfer function for a spindle/tool-holder/tool system

stability of the spindle/tool-holder/tool system as a function of the spindle speed shows this value (See Figure 2) [9, 10, 11]. Chatter and chatter free regions are seen depending on the selected spindle speed range. However, by selecting an axial depth of cut equal to or less than the critical axial depth of cut, a chatter free cutting condition can be achieved. This value is determined for a slotting cut through the relationship:

$$b_{cr} = \frac{1}{(1+\mu).k_{cb}.z_{avg}.\left|Re\{G(j\omega)\}_{neg}\right|_{max}} \, . \tag{4}$$

Table 1 shows values for the specific dynamic cutting coefficient k_{cb} for commonly machined materials.

The spindle cutting performance value S_{pe} determines the amount of the available spindle power, which can be utilized for chip removal. If S_{pe} is less than 1, the available continuous spindle power P_{S1} can only be utilized partially for chip removal. The spindle/tool-holder/tool system will chatter before reaching its maximum continuous spindle power P_{S1}. If S_{pe} is equal to/or greater than 1, the maximum continuous spindle power can be utilized completely for chip removal under no chatter conditions.

As shown in the above equations, the spindle cutting performance S_{pe} is not only influenced by the characteristics of spindle design and the spindle/tool-holder/tool system configuration ($|Re\{G(j\omega)\}_{neg}|_{max}$), but also by the selected cutting parameters such as the chip per tooth, spindle speed and the material properties of the workpiece. To optimize the spindle cutting performance

all of the above influencing parameters have to be taken into consideration. For example, the cutting performance of a given spindle/tool-holder/tool system can be increased from $S_{pe} = 0.7$ to $S_{pe} = 1$ by simply increasing the chip per tooth from 0.13 mm/rev to 0.18 mm/rev.
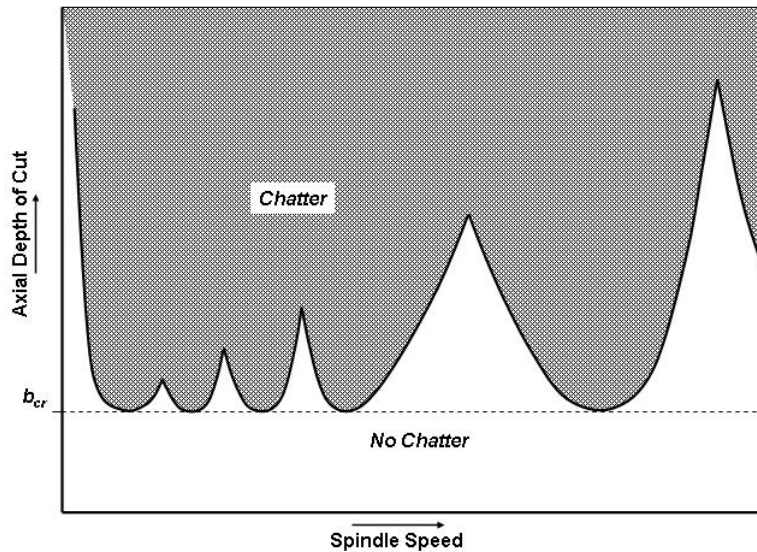

Figure 2: Example of a stability lobe diagram

However, besides changing the technological cutting parameters to increase the cutting performance of a given spindle/tool-holder/tool system, this paper will discuss the influences regarding the conceptual design of milling spindles as well as the configuration of the spindle/tool-holder/tool system to the overall spindle cutting performances. This is demonstrated on an example of a motorized high speed milling spindle which can be configured with different spindle/tool-holder interfaces as well as different types of bearing stiffness.

DYNAMIC MODELING OF MOTORIZED HIGH SPEED MILLING SPINDLES

In order to define the influence of the spindle/tool-holder/tool system configuration of the spindle cutting performance, a Finite Element Model of a motorized 24,000 rpm / P_{S1}=30 kW high speed spindle was modeled by using the FEM-Software ADAMS. Figure 3 shows the conceptual design of the analyzed spindle.

This spindle can be equipped with different configurations depending on the required maximum spindle speed and power. Such configurations are the spindle/tool-holder interfaces, the continuous spindle power, the bearing types (steel-ball or hybrid ceramic bearings) as well as the spindle/machine tool interface.

In general, the modeled spindle is designed with two 70 mm inner-race diameter front bearings mounted back to front, and one 65 mm inner-race diameter tail bearings mounted in floating bushing which is spring loaded against the two front bearings. Additionally, to increase the
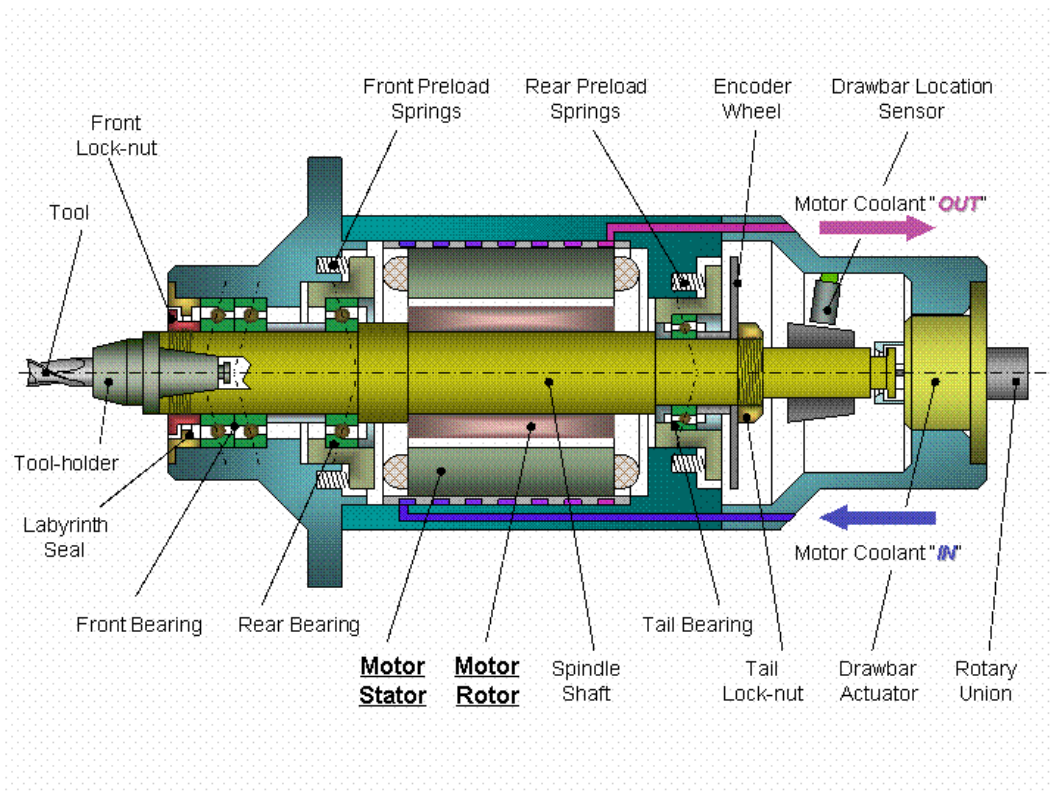
Figure 3: Schematic layout of the analyzed 24,000 rpm, 30 kW high speed spindle.

overall radial spindle shaft stiffness as well as the front bearing axial preload, a rear bearing has been implemented in the front, which is spring loaded against the two front bearings as well. The total axial spindle bearing preload is set at 1800 N. The rotor of an induction-type motor is mounted on the spindle shaft. The continuous power limit P_{S1} is dependent on the heat, which is generated in the stator and rotor. While the generated heat in the stator can be most removed through the water jacket, the heat of the rotor has to pass through the bearings. Due to the temperature limitation of the phenolic ball-cages as well as the required strength of the spindle shaft/rotor interference fit, a maximum continuous spindle power of 30 kW from 5000 to 24,000 rpm cannot be exceeded.

DYNAMIC SPINDLE MODELING WITH FEA

Based on the mechanical model of the spindle design, shown in Figure 3, an FEA model of the spindle shaft was developed using ADAMS software (see Figure 4). The shaft was discreted by multiple beam elements with different cross section geometries. The angular contact bearings were represented by radial and axial linear spring elements with a proper stiffness and damping. The spindle/tool-holder interface was abstracted by two springs at the front and rear of the contact surface as well as by one axial spring element between the spindle and tool-holder, representing the drawbar gripper. Spindle parts, which do not contribute to the spindle stiffness, were simplified as point masses and added onto the shaft to their centers of gravity. Taking advantage of ADAMS, local damping in the springs and the finite elements can be easily counted

and changed. Through applying a virtual impulse force at the modeled tool tip, necessary data for calculating the dynamic compliance of the spindle/tool-holder/tool system can be determined.
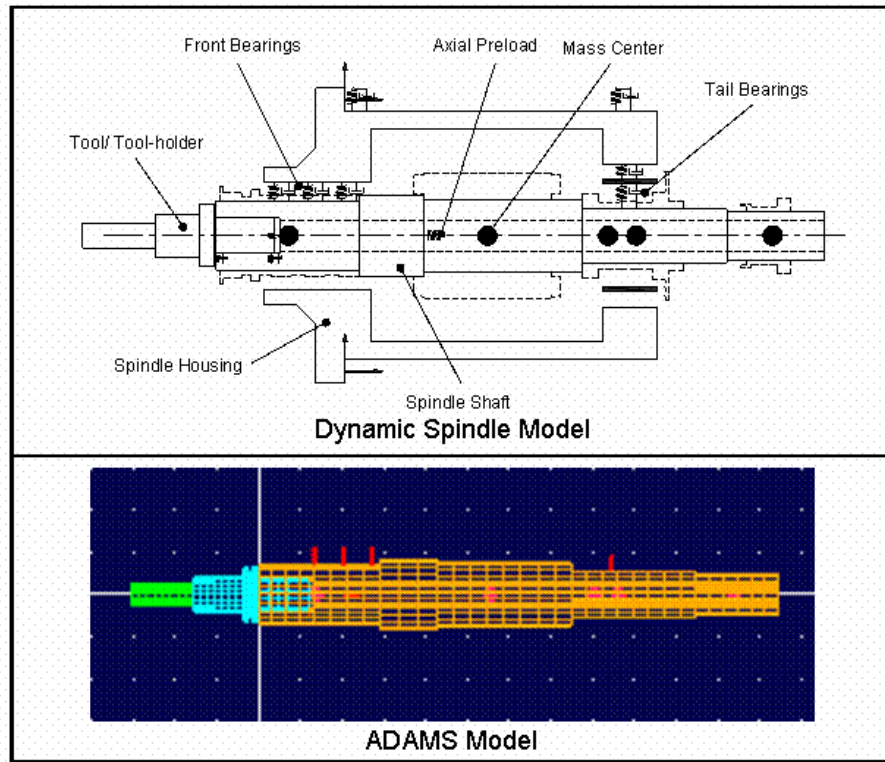

Figure 4: FEA model of the spindle.

DETERMINING THE SPINDLE/TOOL-HOLDER/TOOL SYSTEM DAMPING

Every spindle/tool-holder/tool system consists of multiple mechanical components, which are coupled together and can be represented in a dynamic model as mass, spring and damping elements. While the mass and the spring stiffness determine the natural frequency f_n of the system, the damping element, represented by the damping ratio ξ, governs the resonance increase of the vibration amplitude and with it, the dynamic system stiffness. Therefore, a determination of the local damping ratio ξ or the local viscose damping value c of the spindle/tool-holder/tool system, has paramount importance for modeling the overall dynamic stiffness of a spindle.

Generally, the damping ratio ξ of a dynamic system can be determined by the so-called $\sqrt{2}$-method from the dynamic compliance curve of the spindle/tool-holder/tool system (see Figure 5) [4]. By determining the maximum compliance of the analyzed mode shape $|1/k|_{fR}$ and its multiplication with $1/\sqrt{2}$ the two frequencies f_1 and f_2 can be obtained. With

$$\xi = \frac{f_2 - f_1}{2.f_R} \tag{5}$$
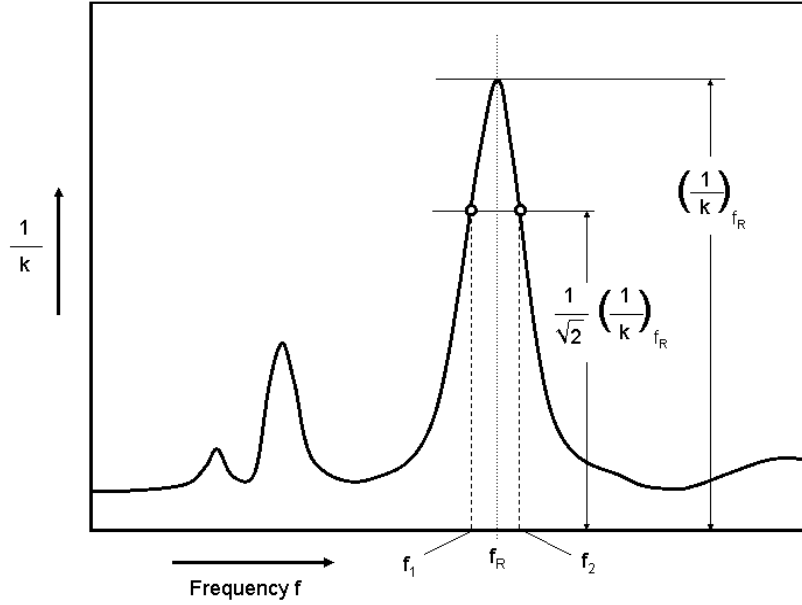
the damping ratio of the analyzed mode can be determined.

Figure 5: √2-method for determining the damping ratio ξ

Like most FEA modeling software, ADAMS requires the viscose damping c, as a model input value. By knowing the damping ratio ξ as well as the natural frequency f_n of the analyzed mode (Real part of the FRF equal 0), the viscose damping value c can be calculated with:
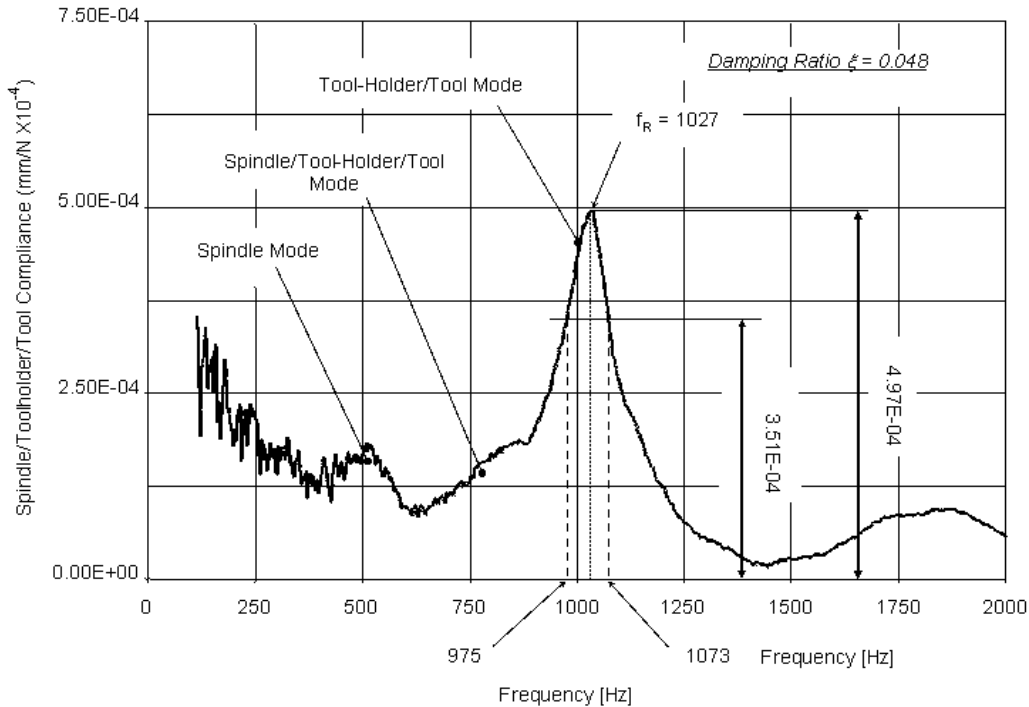
$$c = 2.\xi.\frac{k}{f_n}. \tag{6}$$

This methodology can normally be used for every resonance increase of a measured dynamic compliance curve. For a boundary condition, a judgment must be made as to whether the compliance of the position being examined is, in addition, materially affected by neighboring resonance points. The frequency difference necessary between neighboring resonance frequencies decreases as the damping ratio reduces, i.e. with a narrower spread of the resonance increase.

The determination of the damping ratio ξ for a spindle/tool-holder/tool system from its dynamic compliance curve using the √2-method is only possible for pronounced conditions of single-mass vibrators, i.e. only when the single resonance peaks are occurring far from each other. To determine the damping ratio between the spindle/tool-holder interface, a spreading of the two resonance peaks of the tool-holder/tool assembly and the spindle/tool-holder/tool system has to be established. As a tool/tool-holder assembly, a solid 2-fluted carbide end-mill with a tool diameter of 25.4 mm was implemented into a CAT #40-taper shrink-fit type tool-holder with an overhang of 76 mm (L/D = 3:1). This tool/tool-holder interface has a low dynamic damping ratio and a higher stiffness in comparison to the collet-chuck type tool-holder. Additionally, the total mass of this tool/tool-holder assembly is about 20% less than a collet-chuck type tool-holder assembly, which leads to an additional resonance frequency shift of the tool/tool-holder mode away from the spindle/tool-holder/tool resonance frequency mode. The dynamic compliance function was obtained through measuring the real part (Re{G(jω)}) and the imaginary part

(Im{G(jω)}) of the FRF (frequency response function) using impact excitation at the tip of the tool and applying the equation

$$\frac{1}{k(\omega)} = \sqrt{(\text{Re}\{G(j\omega)\})^2 + (\text{Im}\{G(j\omega)\})^2} \tag{7}$$

to the measured values. The results of these measurements can be seen in Figure 6.

Figure 6: Determining the damping ratio ξ from of the dynamic compliance curve by applying the √2-method

Several prominent modes can be here seen. Analyses through the finite element computation shows that the mode around 512 Hz is the spindle bending mode, referred to in this paper as the spindle/tool-holder/tool mode. The next highest mode at 1027 involves the tool/tool-holder assembly and is referred to as the tool-holder/tool mode. Based on the FRF measurements and the above shown √2-methodology, the damping ratio ξ for the spindle/tool-holder interface can be computed as 0.048.

DETERMINING THE DYNAMIC COMPLIANCES

Modal testing theory has been successfully used for calculating the frequency spectrum of machine tool structures [12]. A frequency spectrum includes the amplitude-frequency characteristic (dynamic compliance) and the phase-frequency characteristic of a system. Frequency characteristic analysis is important to gain an understanding of the dynamic performance of a spindle/tool-holder/tool system especially when the spindle speed has a wide operating range. The dynamic response function can further be used to calculate the stability lobe

diagram to evaluate the dynamic spindle performance. Mathematically, suppose that if the impact force acting on the tool tip is F(t), the displacement response of the tool tip is Y(t), then the dynamic compliance G(jω) of the spindle is defined as

$$G(j\omega) = \frac{\int_0^T Y(t)e^{-jwt}dt}{\int_0^T F(t)e^{-jwt}dt} = \frac{E_Y(j\omega)}{E_F(j\omega)}$$

(8)

where $E_F(j\omega)$ and $E_Y(j\omega)$ are complex energy spectrums of the input force and output displacement. The integrations are the Fourier transform expressions and can be calculated by FFT algorithm [13]. Dividing the complex energy spectrum by the integration time T, we obtain the complex power spectra:

$$S_F(j\omega) = \frac{1}{T}E_F(j\omega)$$

$$S_Y(j\omega) = \frac{1}{T}E_Y(j\omega)$$

(9)

After expansion with the complex conjugate, the dynamic compliance can be expressed as

$$G(j\omega) = \frac{S_Y(j\omega)}{S_F(j\omega)} = \frac{S_Y(j\omega) \cdot S_F^*(j\omega)}{S_F(j\omega) \cdot S_F^*(j\omega)} = \frac{S_{YF}(j\omega)}{S_{FF}(\omega)}$$

$$= \frac{Re\{S_{YF}(j\omega)\} + jIm\{S_{YF}(j\omega)\}}{S_{FF}(\omega)}$$

(10)

where $S_F^*(j\omega)$ is the complex conjugate of $S_F(j\omega)$, $S_{FF}(j\omega)$ is the auto-power spectrum (real), $S_{YF}(j\omega)$ is the cross-power spectrum (complex). The magnitude of $G(j\omega)$ is the dynamic compliance.

MODEL EVALUATION

To evaluate the FEA spindle/tool-holder/tool system model, measurements using impact excitation at the tool tip were performed. Figure 7 shows the dynamic transfer function (real and imaginary part) of the analyzed spindle and the simulation FEA model. About 10 to 20% difference exists due to the omitting of detailed geometry modeling. The purpose of FEA modeling and simulation is not only to define the tendency but also to influence the design parameters (bearing stiffness, spindle/tool-holder interface stiffness and damping, tool geometry, etc.) on the cutting performance; the existing small deviations of the FEA model are insignificant and will not degrade the analytical results.

RESULTS AND DISCUSSION

Generally, the finite element analyses computation of the spindle/tool-holder/tool system shows three dominant mode shapes, which are illustrated in Figure 8. With the given model boundary conditions (stiffness, mass and viscose damping distribution) the first mode, spindle mode,
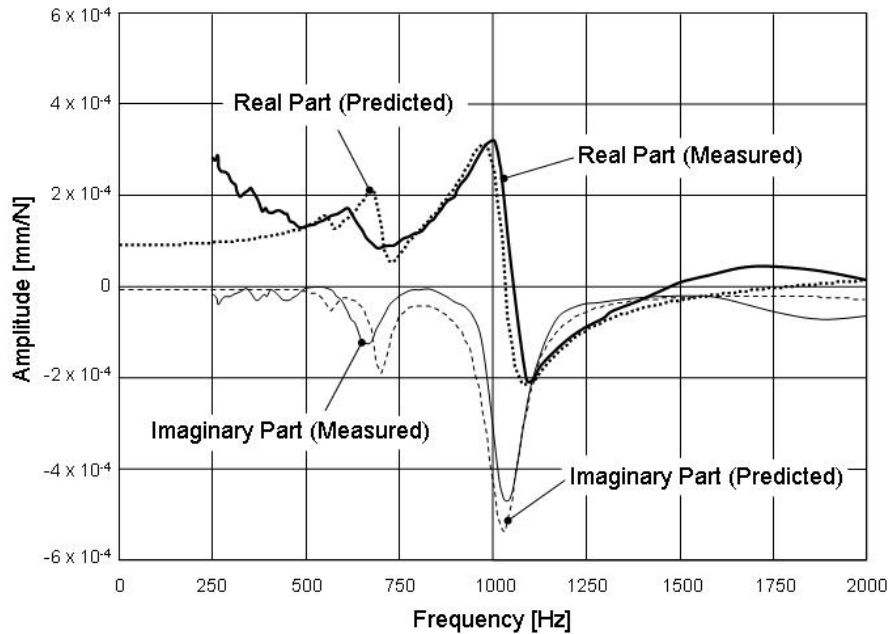
Figure 7: Comparison of the dynamic transfer function between the tap test result and the FEM model simulation

occurred at a resonance frequency of 581 Hz, the second mode, spindle/tool-holder/tool mode, at 720 Hz and the third mode, tool-holder/tool mode, at 1005 Hz. These results where based on a shrink-fit type CAT #40 tool-holder with a 25.4 mm diameter, solid carbide, 2-fluted end mill. The applied stiffness values for the bearings were obtained from the bearing manufacturer, and the stiffness values of the spindle/tool-holder interfaces (CAT #40 HSK 63A and HSK 80F) are based on literature revues [14, 15, 16, 17 and 18]. The selected stiffness and viscose damping values for this case are given in Table 2.

As discussed earlier, the spindle cutting performance is not only determined by the spindle design but also by tool geometry. Figure 9 shows the computed dynamic compliances of the spindle/tool-holder/tool system for a 25.4 and a 19 mm diameter tool with the same overhang of 76 mm. In both cases, the tool-holder/tool mode shape showed the highest dynamic compliance. The transition from a larger to a smaller tool diameter increased the resonance frequency from 1005 to 1087 Hz and its compliance amplitude. Due to the increase of the resonance frequency and the constant damping ratio of the spindle/tool-holder interface (ξ=0.048), the overall width of the resonance peak increases as well.

These results show that the tool diameter has a significant influence on the overall system compliance and the spindle cutting performance. By applying the equations (1 to 4), the spindle cutting performance S_{pe} is for the 19 mm tool diameter 0.39 and for the 25.4 mm tool diameter 0.46. These calculations have been performed for machining aluminum, with a chip load f_z = 0.25mm/rev. Even the predicted maximum negative real part of the FRF for the larger tool was greater than the 19 mm tool diameter (-2 x 10^{-4} mm/N for the 25.4 mm tool and -1.73 x 10^{-4} mm/N for the 19 mm tool), which results in a shallower critical axial depth of cut, the over all material removal rate is higher due to the larger tool diameter. This example shows clearly that

the spindle cutting performance is not only influenced by the spindle design but also by the spindle, tool-holder and tool configuration.
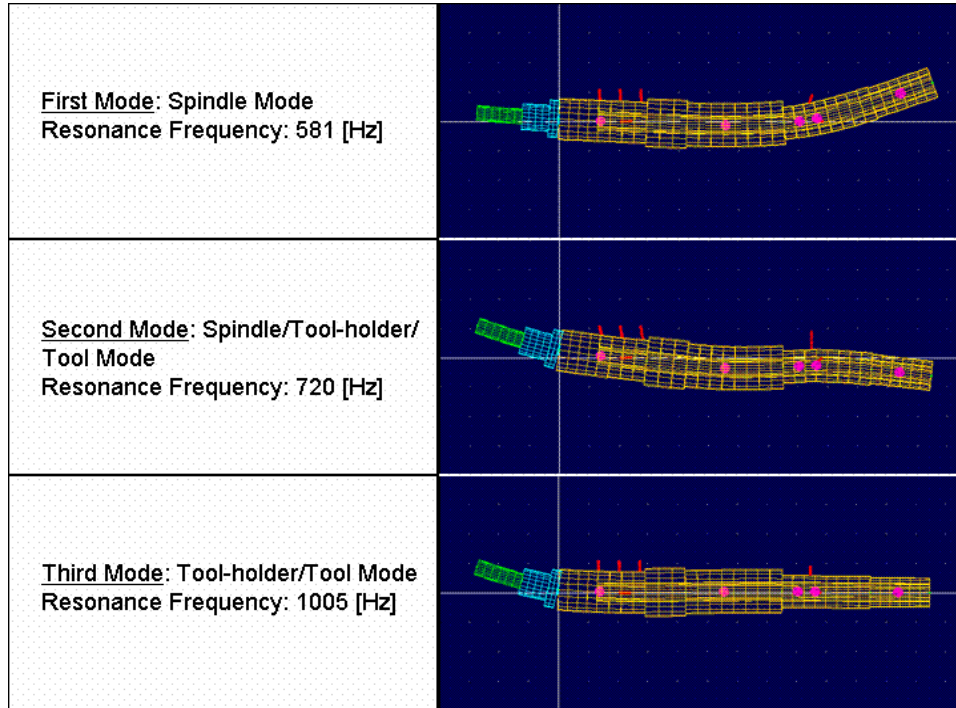

Figure 8: Most dominant mode shapes of the analyzed spindle/tool-holder/tool system

System Component	Stiffness k [N/mm]	Viscose Damping c [Ns/mm]
Spindle/Tool-Holder Interface	Front: 24.0 x 10^5 Rear: 21.6 x 10^5	Front: 0.154 Rear: 0.154
Front Bearing	7.75 x 10^5	0.025
Rear Bearing	7.75 x 10^5	0.025
Tail Bearing	4.1 x 10^5	0.025

Table 2: Stiffness and viscose damping coefficients

The influence of the tool-holder type to the spindle cutting performance has been analyzed through modeling three different spindle/tool-holder interfaces (CAT #40, HSK-63A and HSK-80F) on the above described spindle. All these analyzed interfaces can be implemented on a spindle with a 70 mm inner diameter front bearing. The results of these analyses are shown in Figure 10. As evidenced above, the spindle/tool-holder interface stiffness has a major impact on the compliance of the spindle/tool-holder/tool system. The interface type not only effects the dynamic compliance of the most dominant mode but also all the other modes. Further, the HSK-63A as well as the HSK 80F interface shifts the natural frequency of the tool-holder/tool mode to

a higher frequency due to the increase in the interface stiffness, while the natural frequency of the second mode (spindle/tool-holder/tool mode) remains the same.
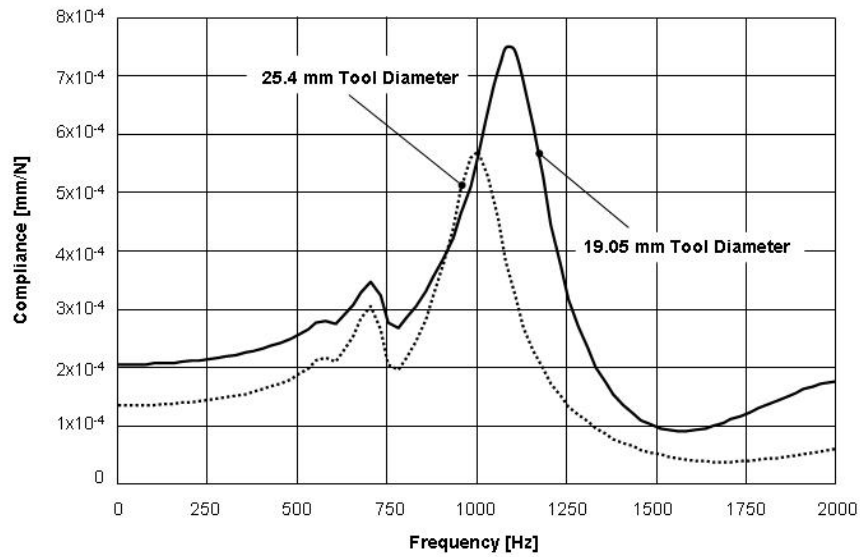

Figure 9: Dynamic compliances of the spindle/tool-holder/tool system for two different tool diameters
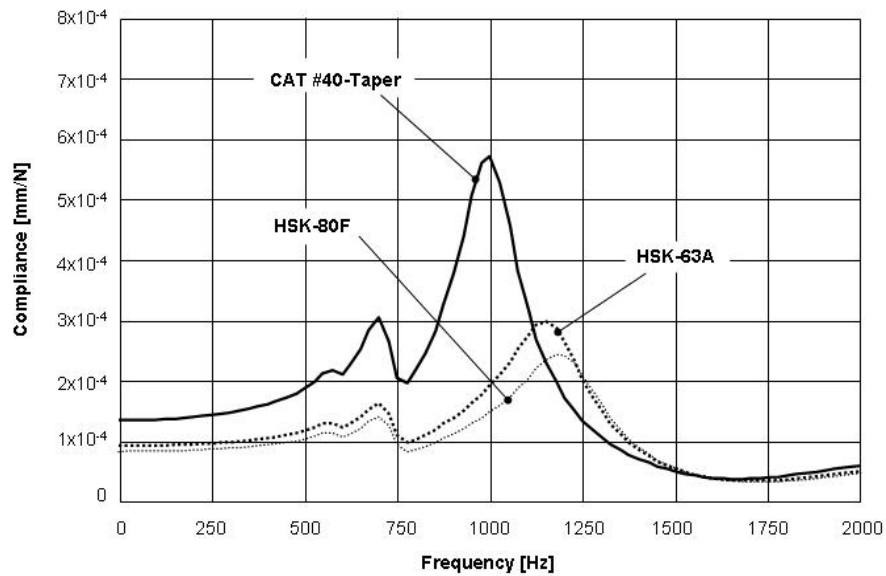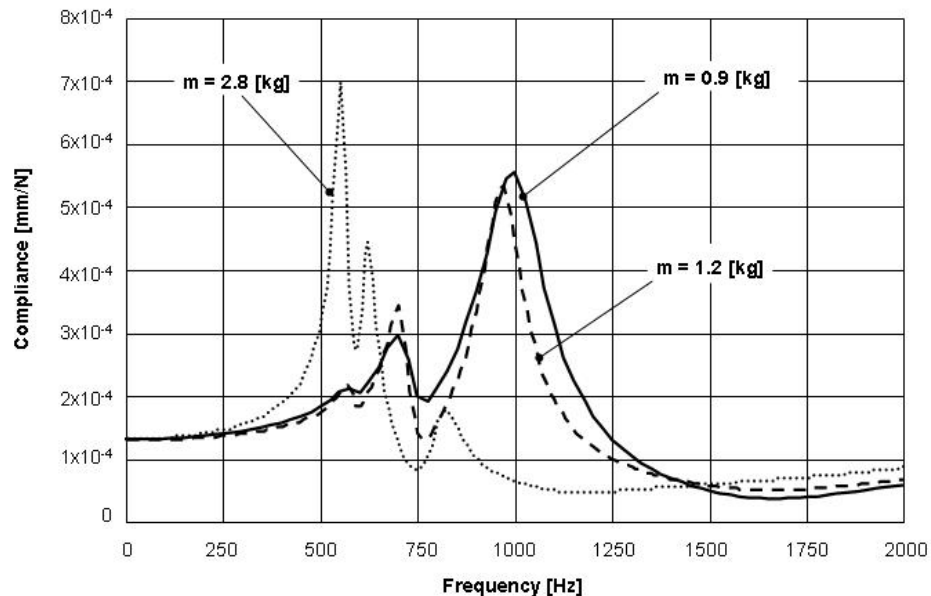

Figure 10: Dynamic compliances of the spindle/tool-holder/tool system for a spindle with CAT #40, HSK 63A and HSK 80F for spindle/tool-holder interface

It is anticipated that by choosing a HSK 63A or HSK 80F interface, a lower dynamic compliance of the tool-holder/tool mode will be seen. Further, the dynamic cutting performance for the above modeled spindle/tool-holder/tool system will increases by 180 % for an HSK 63A interface, due to the smaller predicted maximum negative real part of the FRF (-7.1×10^{-5}). This improvement in the dynamic cutting performances as well as the dynamic stiffness of the tool and tool-holder is mainly caused by the simultaneous fit of the tool-holder flange and the taper to the spindle interface. Additionally, this simultaneous fit also gives the HSK type interface a higher bending moment capability.

Besides the influence of the spindle/tool-holder interface, dynamic FEA computations for determining the influence of the tool-holder mass to the overall dynamic characteristics of the spindle/tool-holder/tool system were performed as well. These analyses were based on three identical CAT #40 type tool-holders with different masses. The first tool-holder represented a shrink-fit type, the second, a collet type (0.3 kg more than the shrink-fit), and the third a hydraulic-chuck type (1.9 kg more than the shrink-fit). All of the analyzed tool-holders were modeled with a 25.4 mm end-mill, which had a tool length (tool tip to tool-holder) of 76 mm. In all three cases the joint stiffness as well as the damping ratio between the tool and tool-holders has been assumed to be the same. The results of these analyses are illustrated in Figure 11. As is evidenced, by increasing the tool-holder mass, the resonance frequency decreases. Especially in the case of the hydraulic-chuck type tool-holder a dramatic frequency shift can be observed. The tool-holder/tool mode shifted from 1005 Hz to 552 Hz, which is below the spindle mode (first mode). In addition, the overall compliance of all modes increased with the tool-holder mass.

Figure 11: Dynamic compliances of the spindle/tool-holder/tool system for three different tool-holder masses

However, the increase of the tool-holder mass has only a minor influence on the spindle cutting performance. Figure 12 shows the real and imaginary parts of the computed dynamic transfer

functions for the shrink-fit and the hydraulic type tool-holders. In the case of the shrink-fit type tool-holder, the third mode (tool-holder/tool mode) dominated the spindle cutting performance (maximum negative real part of the FRF) by increasing the tool-holder mass, while the second mode increases and dominates the overall spindle cutting performance. In both cases, the spindle cutting performance for the analyzed spindle has been determined as $S_{pe} \approx 0.46$.
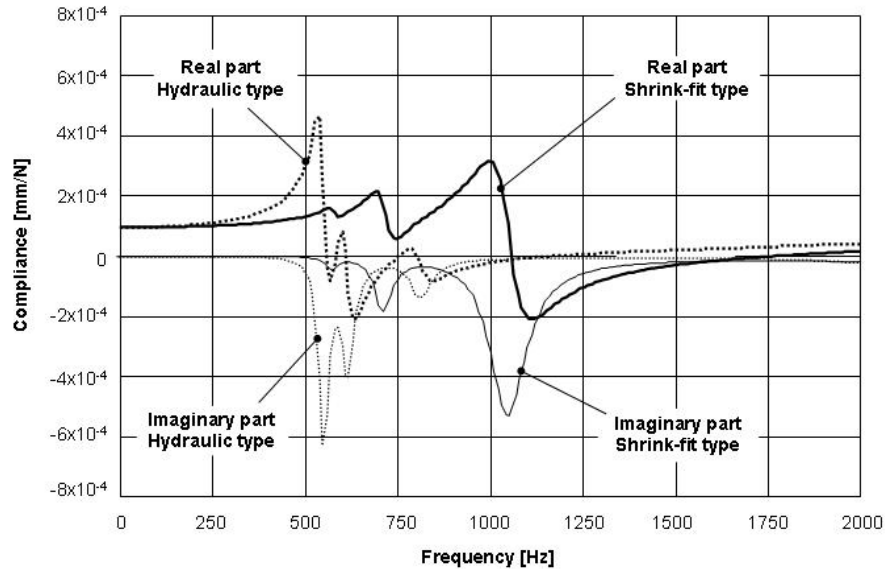

Figure 12: Real and imaginary parts of the computed dynamic transfer functions for a shrink-fit and a hydraulic-chuck type tool-holder

The dynamic mode shape analyses shows that by increasing the tool-holder mass, an amplification of the spindle mode due to the cantilever effect occurs (Figure 13). Additionally, the pronounced vibration conditions of a single-mass or a single spindle component, as it is shown in Figure 7, are no longer effective. The vibrations of the tool-holder/tool mode effect the vibration of the spindle tail and vice-versa. This effect occurs when both resonance frequencies of the tool-holder/tool mode and the spindle mode are approaching each other. As indicated earlier, an increase of the tool-holder mass does not effect the spindle cutting performance but could effect the spindle reliability due to the increased vibration amplitudes of the spindle tail. To avoid machining under chatter conditions, the tooth passing frequency has to approach the most dominant frequency of the spindle/tool-holder/tool system. However, machining under these frequencies will increase the vibration of the spindle tail which can lead to fretting corrosion and/or contact between stationary and rotational spindle parts (encoder wheel, labyrinth seals etc.). The magnitude of these vibrations (spindle tail) can only be determined through the cross transfer function of the spindle/tool-holder/tool system (see Figure 14). In general, it is recommended that to increase spindle reliability, the spindle tail vibration should be lessened through lighter tool/tool-holder masses.

To determine the influence of the spindle bearing stiffness to the overall dynamic behavior of the spindle/tool-holder/tool system, analyses have been performed with the example of two different

angular contact bearing types. The first bearing type was steel ball bearings and the second type, hybrid ceramic. In both cases, the bearing location and the bearing orientation were identical. The applied stiffness values as well as the dynamic compliances are shown in Figure 15. As indicated in the shown figure, a change in the bearing stiffness has only a minor influence on the
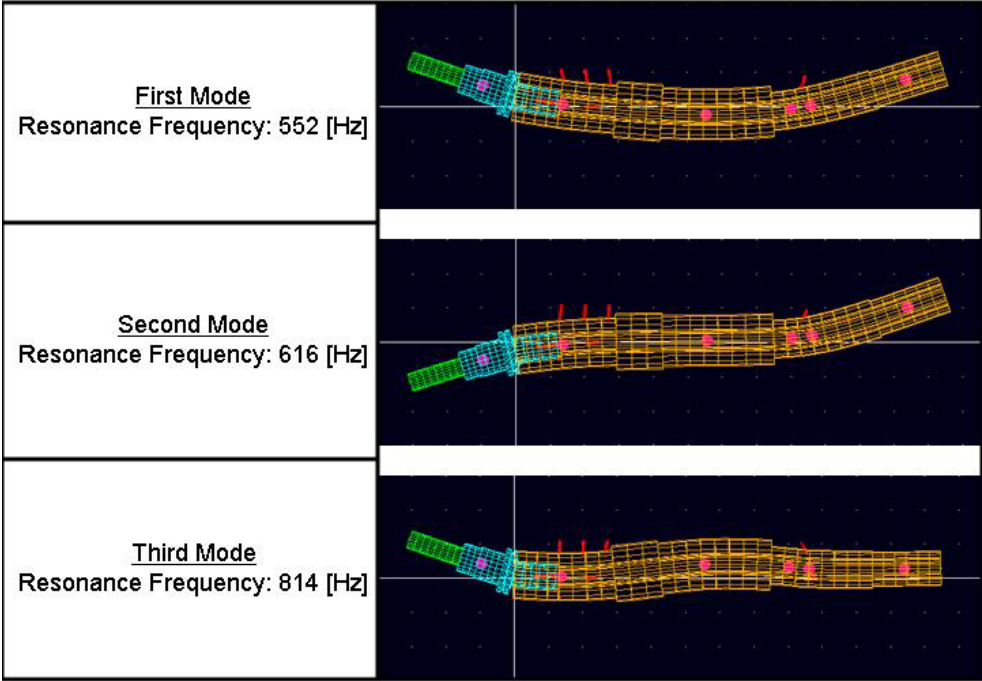

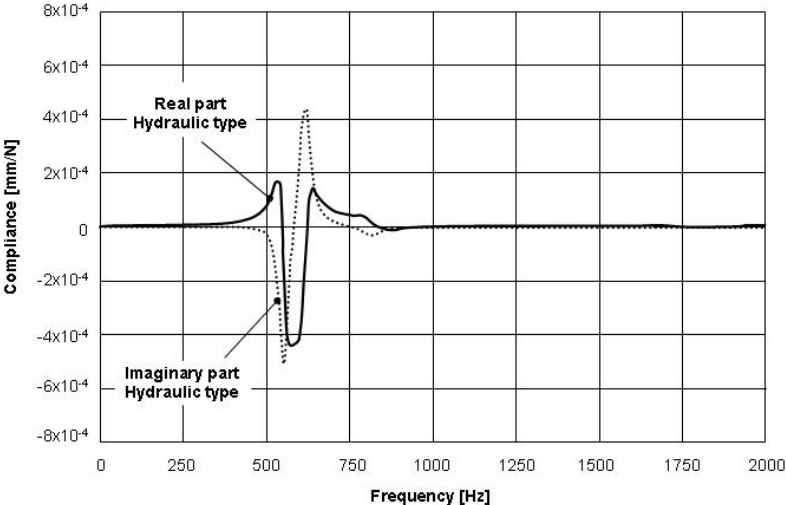Figure 13: Spindle/tool-holder/tool modes for a hydraulic-chuck type tool-holder

Figure 14: Real and imaginary parts of the cross transfer function of the analyzed spindle with the hydraulic-chuck type tool-holder

15

overall system compliance and its cutting performance. The resonance frequency of the spindle/tool-holder/tool mode as well its compliance, increases. Moreover, the most dominant mode (tool-holder/tool mode) is not significantly influenced by the spindle bearing stiffness, therefore, in both cases; the spindle cutting performance remained the same (S_{pe} = 0.46 and 0.47).
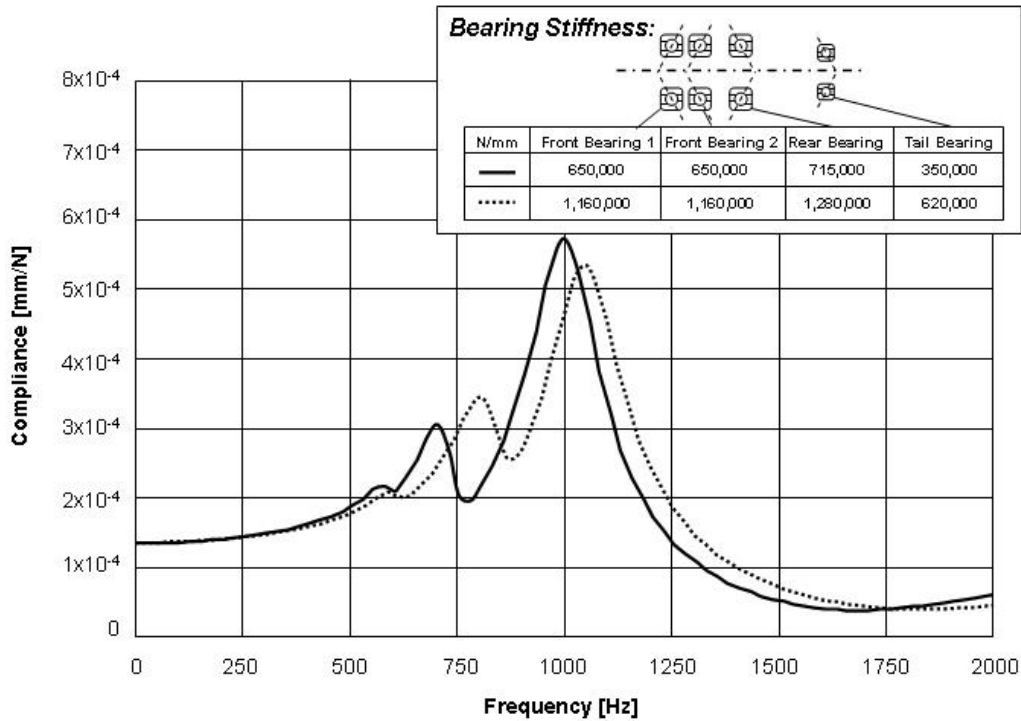

Figure 15: Dynamic compliances of the spindle/tool-holder/tool system for two different bearing types

CONCLUSIONS

A methodology has been established which allows to define the spindle cutting performance for different spindle designs or concepts independently from their application requirements as well as their power and speed characteristics. This methodology was applied on an example of a high speed milling spindle to evaluate the different spindle/tool-holder/tool configurations as well as to determine the influence of the tool-holder and the spindle bearing stiffness to the overall cutting performance. Through a dynamic FEA model of the analyzed spindle the influences of the spindle cutting performance were reached. An analytical approach determined the dynamic compliances as a function of the frequency spectrum. Experimental FRF measurements of this spindle provided the input parameters for this model as well as for model verification. Simulations of different spindle/tool-holder interfaces were explored which showed that the interface stiffness has a dramatic impact on the spindle cutting performance. Additional simulations by varying the tool-holder mass were established as well. Increasing the tool-holder mass allows higher compliance of the tool and the spindle mode. Decreasing the spindle tail

vibration by using lighter tool/tool-holder assembly will increase spindle reliability. Further, the simulations showed that increasing the bearing stiffness has only a minor influence of the spindle cutting performance for the analyzed spindle concept with two front bearing, one rear bearing and one tail bearing arrangement.

REFERENCES

[1]   Tlusty, J.; Koenigsberger, F. In *Specifications and Test of Metal-Cutting Machine Tools*, Proceedings of the Conference 19th and 20th, University of Manchester, Institute of Science and Technology (UMIST), Feb 19-20, 1970; Revell and George Limited: Manchester; Vol. 1.

[2]   *Cutting tests for determining the dynamic machine tool behavior,* BAS-Standard, Sweden, 1970, AB BORFORS; ALFA-LAVAL AB; ASEA; SAAB-SCANIA.

[3]   *Machine Test Book-Records of Spindle Test*, 1998, CINCINNATI MACHINE.

[4]   Weck, M. Dynamisches Verhalten von Werkzeugmachinen. In *Werkzeugmanschinen, Fertigungssysteme, Messtechnische Untersuchung und Beurteilung*; VDI-Verlag GmbH: Dueselldorf, 1992; Vol. 4, 269-282.

[5]   Weck, M.; Teipel, K. In *Dynamisches Verhalten spanender Werkzeugmaschinen*; Springer-Verlag: Berlin, Heidelberg, New York, 1977.

[6]   Tlusty, J.; Smith, S.; Zamudio, C. In *Evaluation of Cutting Performance of Machining Centers*, Annals of the CIRP **1991**, 40/1, 405-410.

[7]   Smith, S.; Winfough, W.; Young, K.; Hally, J. In *The Effect of Dynamic Consistency in Spindles on Cutting Performance*, Proceeding of the ASME Manufacturing Engineering Division 2000, MED-Vol. 11, 927-933.

[8]   Tlusty, J. Handbook of High Speed Machining Technology, In *Machine Dynamics*; R.I. King, ed., Chapman and Hall, New York.

[9]   Altintas, Y.; Budak, E. In *Analytical Prediction of Stability Lobes in Milling*, Annals of the CIRP 1995, 44/1, 357-362.

[10]   Smith, S.; Tlusty, J. In *Update on High-Speed Milling Dynamics*, Transaction of the ASME Journal of Engineering for Industry 1990, 112, 142-149.

[11]   Tlusty, J.; Zaton, W.; Ismail, F. In *Stability Lobes in Milling*, Annals of the CIRP 1983, 32/1, 309-313.

[12]   Ewins, D.J. Theory and Practice, In *Modal Testing*; John Wiley & Sons, Inc.: New York, 1984.

[13]   Brigham, E.O. In *The Fast Fourier Transform and its Applications*; Prentice Hall Inc.: Englewood Cliffs, NJ, 1988.

[14]   Erstellung einer technischen Richtlinie fuer Holschaftkegel-Werkzeuge, Report of the 6th committee meeting, WZL, Sep 2001; RWTH-Aachen, Germany.

[15]   Agapiou, J.; Rivin, E.; Xie, C. *In Toolholder/Spindle Interfaces for CNC Machine Tools*, Annals of CIRP 1995, 44/1, 383-387.

[16]   Weck, M.; Schubert, I. In *New Interface Machine/Tool: Hollow Shank*, Annals of the CIRP 1994, 43/1, 345-348.

[17]   Schmitz, T. In *Predicting High-Speed Machining Dynamics by Substructure Analysis*, Annals of the CIRP 2000, 49/1, 303-308.

[18]   Ferreira, J.; Ewins, D. In *Nonlinear Reacceptance Coupling Approach Based on Describing Functions*, Proceeding of the 14th International Modal Analysis Conference, 1995, Dearborn, MI, 1034-1040.